IDEAL TAPER PREDICTION FOR BILLET CASTING

Chunsheng Li and Brian G. Thomas
Mechanical and Industrial Engineering Department
University of Illinois at Urbana-Champaign
1206 W. Green St., Urbana, IL 61801
Tel.: 217 244 2859, 217 333 6919
E-mail: cli1@uiuc.edu, bgthomas@uiuc.edu

Key words: Taper, Bulging, Billet, Elastic-viscoplastic, Finite Element, Thermal-mechanical Model

INTRODUCTION

Mold taper is an important control parameter in the continuous casting of steel billets. Properly tapered mold walls compensate for shrinkage of the solidifying strand to maintain good contact and heat transfer between the mold wall and shell surface without exerting extra force on the hot and weak shell. The amount of taper needed varies with steel composition and casting conditions, such as mold length, casting speed, and type of lubrication. Inadequate mold taper leaves an air gap between the mold wall and shell surface which leads to a hotter and thinner shell within the mold. Ferrostatic pressure from the liquid core will bulge the weak shell within and out of the mold and even break out the shell in extreme situations. Excessive taper exerts extra load on the solidifying shell and increases dragging friction. Transverse cracks, shell buckling or even shell jamming and breakouts may occur. Past efforts conducted to assist mold taper prediction includes mathematical models to calculate thermal shrinkage of the steel billet [1-3] and thermal distortion of the mold [3-6]. These previous investigations assume optimal taper should match the shell shrinkage, presuming this should produce good heat transfer across the interfacial layer between mold wall and billet surface at the face center along the mold axial direction. Corner effects have received little attention.

The first objective of this work is to investigate the criteria for taper optimization by considering conditions at the billet corner needed to avoid cracks and defects both within and below the mold assuming the good mold taper is already provided along the face center. Current billet molds often adopt simple flat walls, which produce inadequate taper in the central portion down the mold. This will lead to gap formation near the corner and off-corner hot spots leading to longitudinal corner cracks or bulging and sub-surface off-corner cracks [7] when the billet leaves the mold. Even if the taper design is optimized down the mold to match shrinkage of the face center, a gap can still form near the corners. This optimization task itself is difficult because the shell will always bulge under ferrostatic pressure towards the mold walls as taper is not perfect. On the other hand, if the taper is designed to prevent any air gap around the billet parameter, the cold and strong corner will prevent the shell from bulging when it leaves the mold [8]. However, the billet corner will cool faster than the face center if

the heat transfer rate is equal around the perimeter of the billet [8] due to 2D heat transfer near the corner. Moreover, the extra taper needed will likely increase friction jamming and transverse cracks between the mold and the billet if it does not match perfectly. Thus, this strategy too will be questioned by investigation in this work. Since neither of the design methods is perfect, a third strategy emerges. The optimal taper should avoid casting defects by avoiding air gaps along the billet face center to ensure good heat transfer and also leave some air gap near the corner to make the surface temperature near the corner equal to the surface temperature at the center.

The criteria for how to chose optimal taper is studied in this work, based on simulations of the thermal-mechanical behavior of billets with the three types of mold configuration producing hot corner, cold corner and equal surface temperature around the perimeter. Optimal taper profiles are then predicted as a function of casting speed, using a computational model fit to match billet heat flux measurements.

MODEL DESCRIPTION

For this study, a transient, thermal-elastic-visco-plastic finite element model, CON2D [9, 10], has been developed to follow the thermal and mechanical behavior of a section of the solidifying steel shell, as it moves down the mold at the casting speed. It is applied in this work to simulate temperature, stress, strain and deformation in a 2D section of a continuous casting billet aiming to achieve a realistic steel shell cast under ideal conditions which generate monotonic cooling in the mold and neither sudden cooling nor reheating below the mold.

Modeling Domain

The modeling domain is a L-shaped region in one quarter of a transverse section through a continuous cast steel billet, assuming symmetrical temperature and stress distributions about the billet center lines, as shown in Fig. (1a). Fig. (1b) and (1c) show the mesh of the 3-node triangle elements used for heat transfer analysis and 6-node mesh of triangle elements for stress analysis, respectively.

This domain includes the entire solid shell in the upper portion of the caster, but ignores some of the liquid near the billet center to save on computation requirements. Smaller size elements, 0.1mm, are used near the surface to produce more accurate thermal stress/strain prediction during the initial solidification period. Larger size elements, 1.0mm, are used near the center to reduce computational cost substantially, without sacrificing much accuracy.

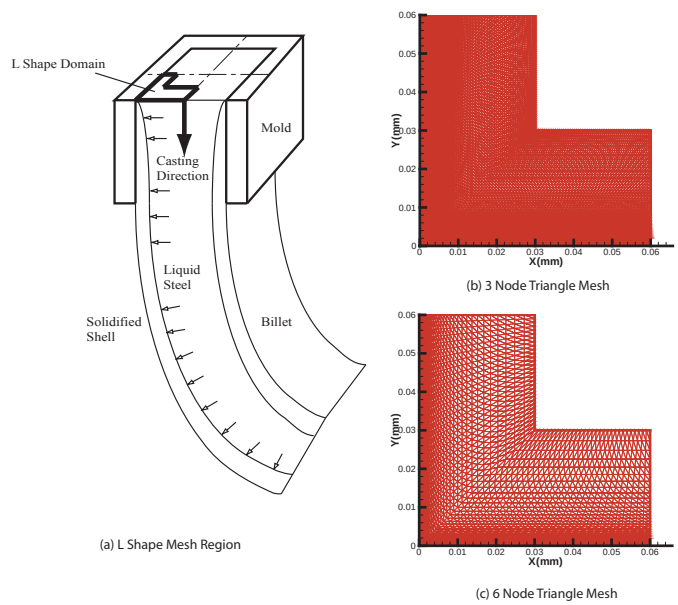

Figure 1: Schematic of 2D Domain and Meshes

Heat Transfer Model

The heat transfer model solves the 2D transient conduction equation, using a fixed Lagrangian grid of 3-node triangles. Latent heat is evaluated using the spatial averaging technique suggested by Lemmon [11]. Axial heat conduction is ignored. A non-equilibrium phase transformation model for plain carbon steels suggested by WON [12] is incorporated to produce realistic phase fraction evolution between solidus and liquidus temperatures. Fig. (2) shows the fractions of solid phases and liquid for 0.27%C carbon steel, which is investigated in this work. The steel composition and important temperatures are shown in Table I.

Table I: Material Details

Steel Composition (wt%)	0.27C, 1.52Mn, 0.34Si, 0.015S, 0.012P
Liquidus Temperature (°C)	1500.72
70% Solid Temperature (°C)	1477.02
90% Solid Temperature (°C)	1459.90
Solidus Temperature (°C)	1411.79
Austenite→α-Ferrite Starting Temperature (°C)	781.36
Eutectoid Temperature (°C)	711.22

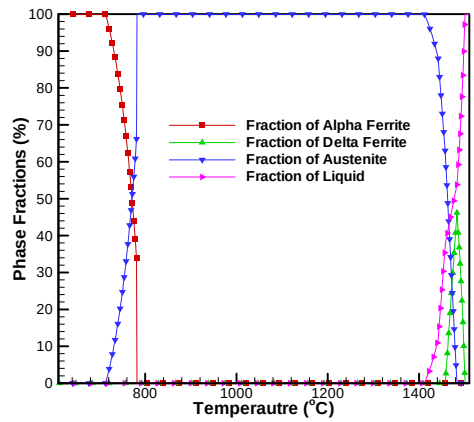

Figure 2: Phase Fraction versus Temperature for Steel with 0.27%C, 1.52%Mn, 0.015%S, 0.012%P, and 0.34%Si

Stress Model

Starting with stress-free liquid at the meniscus, the stress model calculates the evolution of stresses, strains, and displacements by interpolating the thermal loads onto a fixed mesh of 6-node triangle finite elements [9]. The elastic strain rate vector, $\{\dot{\varepsilon}_e\}$, is related to the total strain vector, $\{\dot{\varepsilon}\}$, via:

$$\{\dot{\varepsilon}_e\} = \{\dot{\varepsilon}\} - \{\dot{\varepsilon}_T\} - \{\dot{\varepsilon}_{in}\} - \{\dot{\varepsilon}_f\} \tag{1}$$

Where $\{\dot{\varepsilon}_T\}$ is the thermal strain rate, $\{\dot{\varepsilon}_{in}\}$ is the inelastic strain rate including creep and plasticity, $\{\dot{\varepsilon}_f\}$ is the pseudo-strain rate representing fluid flow of the liquid. Friction between the mold and shell surface is ignored by assuming that there is no excessive mold taper in this work. Thermal strain is calculated from the temperature changes calculated by the heat transfer model and from the unified state TLE, thermal linear expansion, function which reflects the volume change of materials under temperature change and phase transformation. The thermal strain can be expressed by:

$$\{\varepsilon_{th}\} = \left(TLE(T) - TLE(T_0)\right)\{1 \quad 1 \quad 0 \quad 1\}^T \quad where \quad TLE(T) = \sqrt[3]{\rho(T_0)/\rho(T)} - 1 \tag{2}$$

A realistic unified elastic-visco-plastic model III of Kozlowski [13] for the austenite phase and an enhanced power law model [14] for the δ-ferrite phase are adopted in this work. These models were developed to match tensile test measurements of Peter Wray [15, 16] and creep data of Suzuki [17] over a range of strain rates, temperature, and carbon contents to model austenite/ferrite under continuous casting conditions. Fig. (3) compares the constitutive model with measured stresses under 5% strain and 2.8×10^{-5} 1/sec. and 2.3×10^{-2} 1/sec. strain rate from 1200 °C to 1600 °C. Predicted stresses match the measurements decently.

The liquid elements are generally given no special treatment regarding material properties and finite element assembly. The only difference between solid and liquid is choosing a constitutive equation that provides an extremely rapid creep rate in the liquid phase, which is shown in Eq. (3), to enforce negligible liquid strength and stress.

$$\dot{\bar{\varepsilon}}_{flow} = \begin{cases} 10^8\left(|\bar{\sigma}| - \sigma_{yield}\right)^5 & |\bar{\sigma}| > \sigma_{yield} \\ 0 & |\bar{\sigma}| \le \sigma_{yield} \end{cases} \quad where \quad \sigma_{yield} = 0.01MPa \tag{3}$$

Mold constraints are applied to prevent the billet from expanding freely because of the ferrostatic pressure. Care is taken not to apply non-physical restraint to limit shell shrinkage. An efficient contact algorithm described elsewhere [9] is used to achieve this goal. Mold distortion, ΔW_{mold} (mm), is calculated as a function of distance down the mold by:

$$\Delta W_{mold} = \alpha_{mold} \cdot \frac{W}{2} \cdot \left(\bar{T} - \bar{T}_0\right) \tag{4}$$

$\bar{T}$ is the average temperature through the mold wall thickness as a function of the distance below mold exit. $\bar{T}_0$ is the average mold wall temperature where the solid shell begins, α_{mold} is the thermal expansion coefficient of the copper mold tube, and W is section width.

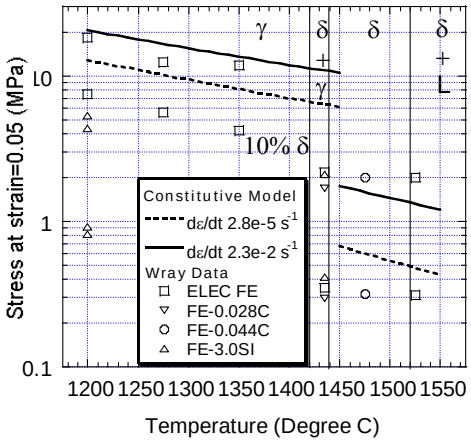

Figure 3: Comparison of Model Predicted and Measured (Wray [15, 16]) Stresses

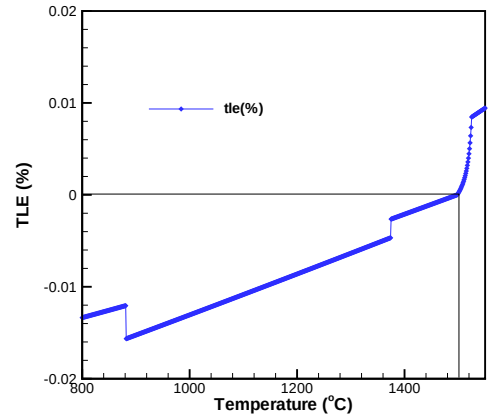

Figure 4: Thermal Linear Expansion for 0:27%wtC Plain Carbon Steel

Temperature dependent material properties are used in this work to capture the thermal-mechanical behavior of the steel as realistically as possible. The temperature dependent functions of thermal conductivity and enthalpy developed by Harste [18] are adopted. Density was assumed constant at 7500 Kg/m^3 in this work, in order to maintain constant mass. Fig. (9) shows the thermal linear expansion curve for 0.27%wtC plain carbon steel used in this study, which is obtained from solid phase density measurements compiled by R. K. Harste [18] and Jablonka [19] and liquid density measurements by Jimbo and Cramb [20] via Eq. (5), where the arbitrary reference state T_0 is chosen to be the solidus temperature.

$$TLE = \sqrt[3]{\frac{\rho(T_0)}{\rho(T)}} - 1 \tag{5}$$

The details the steel properties including the conductivity, enthalpy as well as elastic modulus can be found elsewhere [21].

HOT TEAR FAILURE CRITERIA

To evaluate which taper is optimal in order to avoid hot-tear cracks, a criterion is need to quantitatively predict when hot-tear cracks begin to initiate. A simple empirical critical strain function, ε_c, fitted by Won [22] from many measurements, was adopted in this work as a fracture criterion given in Eq. (6). Hot tear cracks form if the thick dendrites in the brittle temperature range, ΔT_B [22], prevent the surrounding liquid from compensating the contraction of interdendritic liquid and solid expansion. Cracks are predicted when damage strain, ε_{damage}, exceeds the critical strain, ε_c.

$$\varepsilon_{damage} \geq \varepsilon_c \quad where \quad \varepsilon_{damage} = \sum_{f_s=0.9}^{f_s=0.99} \Delta\varepsilon_{flow\_hoop} \quad and \quad \varepsilon_c = \frac{0.02821}{\dot{\varepsilon}^{0.3131} \Delta T_B^{\,0.8638}} \tag{6}$$

Damage strain is defined as the flow strain accumulated within the brittle temperature range, calculated during the post-processing phase. The damage strain component chosen for comparison is taken perpendicular to the dendrite growth direction, which is along the "hoop" direction, so named because it is tangential to the surface of the solidifying shell. The brittle temperature range, ΔT_B is 9 ^{o}C for this grade and $\dot{\varepsilon}$ is strain rate.

MODEL VALIDATION

CON2D was first validated by comparing to an analytical solution of thermal stress evolution in an unconstrained solidifying plate proposed by Weiner and Boley [23]. The material in this problem has elastic-perfect plastic behavior whose yield stress linearly drops with temperature. In CON2D, this constitutive equation was transformed into a computationally more challenging form of the highly nonlinear creep function of Eq. (3). A very narrow mushy region was used to approximate the single melting temperature assumed by Boley and Weiner. CON2D matched both the temperature and thermal stress analytical profiles as closely as desired by refining the mesh. Details of this validation are described elsewhere [8]. Matching this analytical solution provides the validation of CON2D finite element model as well as the mesh size and the time step increment, which are used in this work.

Then, CON2D was applied to predict the casting speed limits preventing the off-corner sub-surface hot tear cracks due to excessive sub-mold bulging of steel billets [8]. The predicted casting speed limits varies from 1.0 m/min for a 600 mm long, 250 mm square mold to 6.0 m/min for a 1000 mm long, 120 mm square mold. These speeds match plant practice [24]. Hot tear cracks are predicted at the location 12 ~ 15 mm to the billet corner, 10 ~ 15 mm beneath the billet surface under the casting speeds beyond the predicted casting speed limits. These also match the location of off-corner sub-surface hot cracks found from breakout shell [8]. Thus, the ability to predict hot-tear cracks near solidification front of CON2D is validated.

Finally, CON2D was applied to simulate a plant trial conducted at POSCO, Pohang works, South Korea, for a 120 mm square section billet of 0.04%C steel cast at 2.2 m/min. A single linear taper of 0.75%/m was used during the trial. FeS tracer was suddenly added into the liquid pool during steady state casting to measured the solid shell growth. CON2D matched the heat flux and mold wall temperature measurements along the billet face center. A 5 mm solid shell is measured near face center from the transverse section taken at 285 mm below meniscus, which corresponds to 7.8 sec. of simulation time [25]. Shell thickness was defined in CON2D as the isotherm corresponding to the coherency temperature, assumed to be 70% of solid. A 4 mm shell thickness was predicted by CON2D at 285 mm below meniscus. The general solid shell shape predicted and measured match quite reasonably except that the agreement of corner thinning is only qualitative, since no round corner is included in CON2D. This agreement validates the fully coupled thermal-stress model CON2D, used here.

SIMULATION CONFIGURATION

Traditionally, it is assumed that optimal taper should exactly match shell shrinkage everywhere around the mold perimeter. However, corner effects are complex and providing proper taper to match corner shrinkage is very important. To understand the thermal-mechanical behavior of the billet especially at corner, three different mold configurations have been simulated under two casting speeds, 2.2 m/min and 4.4 m/min, which are within the normal industrial operation range. The first configuration is taken from a plant trial conducted at POSCO, Pohang works, South Korea [7]. A single linear taper of 0.75%/m is used during this trial. The second configuration assumes perfect contact between mold wall and shell surface around the billet perimeter. This implies uniform heat flux around the mold perimeter. This is an idealized condition that requires a complex mold wall surface following the shell shrinkage everywhere from the meniscus to the mold exit. The third configuration is a different idealized mold wall shape, which produces uniform surface temperature

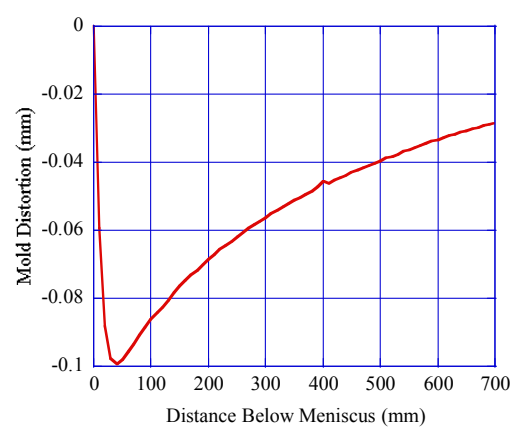

Figure 5: Mold Distortion for 2D Simulation

around the billet perimeter. The actual shape is unknown before the simulation is conducted. It can be extracted by backward calculation according to the heat flux function around the billet surface and air gap properties.

Although these mold configurations would be very difficult to implement in practice, the conditions are easy to achieve in the model. They are simply three different thermal boundary conditions applied at the billet surface: 1) heat transfer resistor model between shell surface and mold wall which requires fully coupled thermal-stress simulation, 2) uniform heat flux around the billet perimeter as a function of casting time, and 3) uniform surface temperature around the billet parameter as a function of casting time. Each is discussed in turn.

1) Heat Transfer Resistor Model (0.75%/m Taper)

The first configuration simulates a realistic operating practice of flat mold walls with a fixed taper of 0.75%/m. Fig. (6) shows the heat transfer resistor model assumed between the mold wall and the shell surface. The values of the parameters are given in Table II.

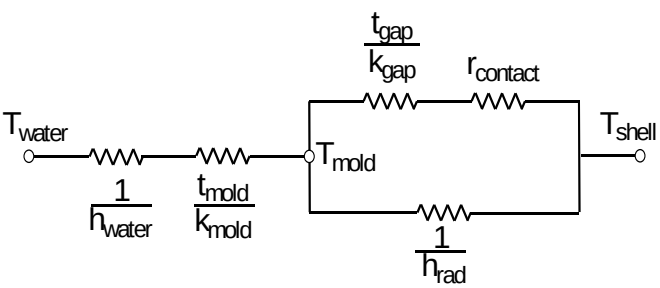

Figure 6: Schematic of Thermal Resistor Model of the Interface Between Mold and Billet

Table II: Parameters of the Interface Model

Cooling Water Heat Transfer Coefficient, h_{water} (W/m^{2}K)	22,000 ~ 25,000
Cooling Water Temperature, T_{water} (^{o}C)	30 ~ 42
Mold Wall Thickness, t_{mold} (mm)	6
Mold Wall Conductivity, k_{mold} (W/mK)	360
Gap Conductivity, k_{gap} (W/mK)	0.1
Contact Resistance, $r_{contact}$ (m^{2}K/W)	6×10^{-4}
Mold Wall Emissivity	0.5
Steel Emissivity	0.8

The values of cooling water temperature and its heat transfer coefficient vary from meniscus to mold exit. The actual profiles are taken from a more advanced heat transfer model, CON1D [26]. The contact resistance differs from its physical value between steel and copper because it also includes the effect of oscillation marks is included. The heat extraction rate is mainly determined by the gap in the interfacial layer, which further depends on the instantaneous mold wall distortion and the shrinkage of the shell. Mold distortion from Eq. (4) is given in Fig. (5).

The shrinkage of the shell is taken from the mechanical analysis. Since the temperature and stress/strain distributions depended on each other and are unknown in prior, a fully coupled simulation procedure as given in Fig. (7) is needed. At each time step, the gap size from the previous time step is used to estimate the heat transfer rate and the heat transfer equations are solved. Then, the mechanical model is

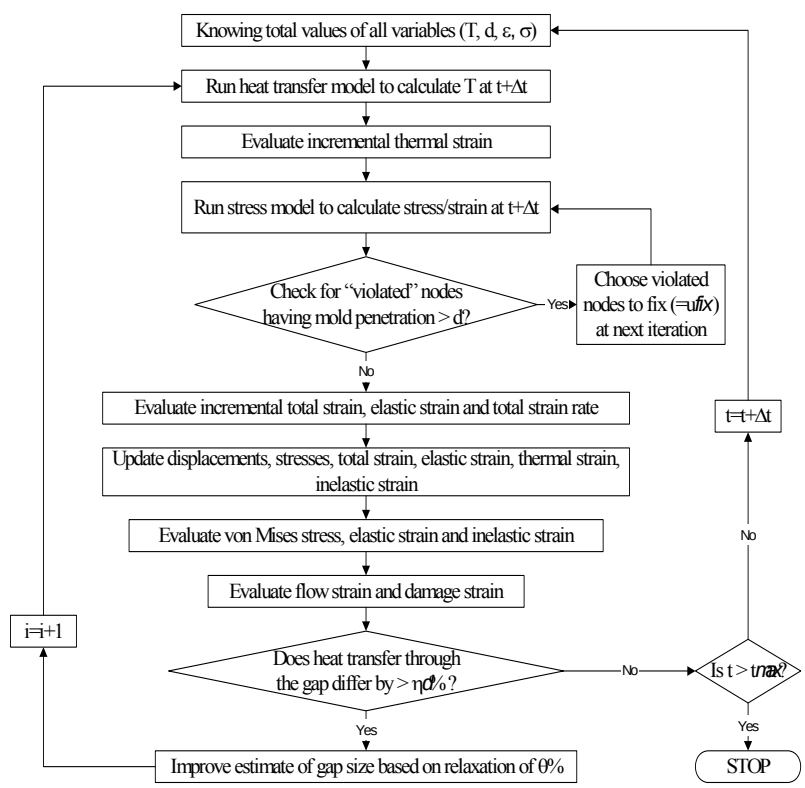

Figure 7: Schematic of the Fully Coupled Simulation of CON2D

solved based on the new temperature distribution to give out a new gap. The two-step procedure is repeated until the gap sizes from two successive iterations are close enough.

2) Uniform Heat Flux Around Mold Perimeter Model

The instantaneous interfacial heat flux profile down the mold in this case is obtained by differentiating the average heat flux profile, fitted from average heat flux data points measured by many investigators [24, 27-31]. In addition, the instantaneous heat flux function is compared with instantaneous heat flux measurements by Samarasekera and coworkers [32]. Eqs. (7) and (8) show the fitted average and instantaneous heat flux functions. Figs. (8) and (9) compare the average and instantaneous heat flux curve against the measurements.

$$\bar{q}\left(MW/m^3\right) = 13t\left(\sec.\right)^{-1}\left[\left(t\left(\sec.\right)+1\right)^{0.5}-1\right] \tag{7}$$

$$q\left(MW/m^3\right) = 6.5\left(t\left(\sec.\right)+1\right)^{-0.5} \tag{8}$$

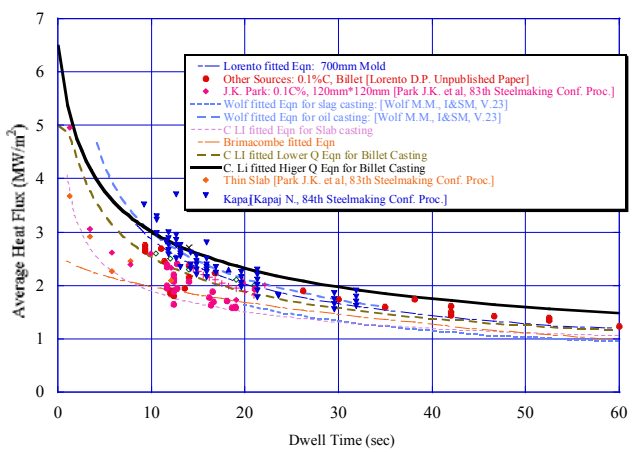

Figure 8: Measured Average Heat Flux and Fitted Functions

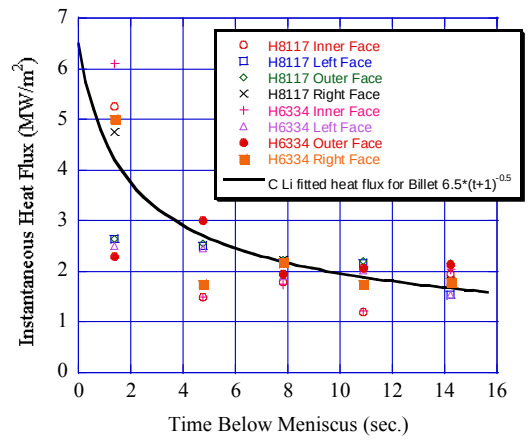

Figure 9: Instantaneous Heat Flux Curve

3) Uniform Surface Temperature Around Mold Perimeter Model

The third mold configuration fixes the surface temperature to be uniform around the mold perimeter, and is shown in Fig. (10). This profile is identical to the surface temperature profile generated down the face center while the heat flux function (Eq. (8)) is applied.

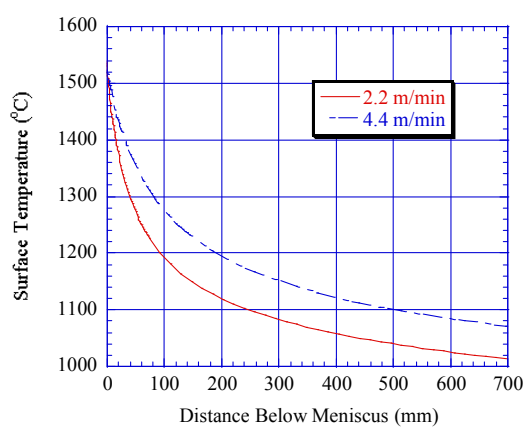

Figure 10: Uniform Surface Temperature

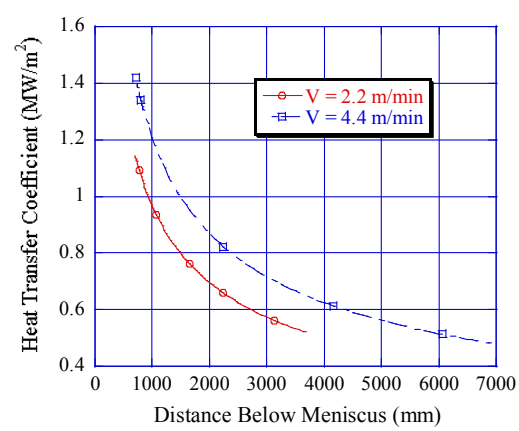

Figure 11: Heat Transfer Coefficient In Spray Zone

Secondary Cooling Pattern

After the billet exits the mold, it enters the secondary cooling region. A heat convection coefficient function suggested by Nozaki [33] is adopted in this work. The secondary cooling rate in this work is designed to minimize the sudden surface temperature change at the face center when the billet leaves the mold. Fig. (11) shows the heat transfer coefficient profile for both casting speeds.

BILLET BEHAVIOR FOR DIFFERENT MOLD CONFIGURATIONS

CON2D is applied to predict thermal-mechanical behavior of billets cast under the 3 different mold configurations described previously. The optimal taper strategy will be chosen based on avoiding both in-mold and below-mold cracks as well as excessive bulging. The simulation results are evaluated according to the effects on the shell growth, sub-mold bulging, and transverse corner cracks as well as longitudinal off-corner sub-surface cracks.

Surface Temperature and Shell Growth

Fig. (12) shows the temperature contours at the mold exit for the three types of mold configurations. The liquidus at 1500.72 ^{o}C and solidus at 1411.79 ^{o}C isothermals mark the shell growth at mold exit.

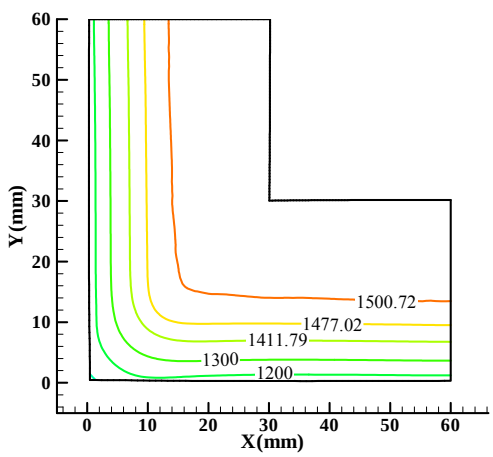

(a) 2.2m/min, 0.75% Linear Taper

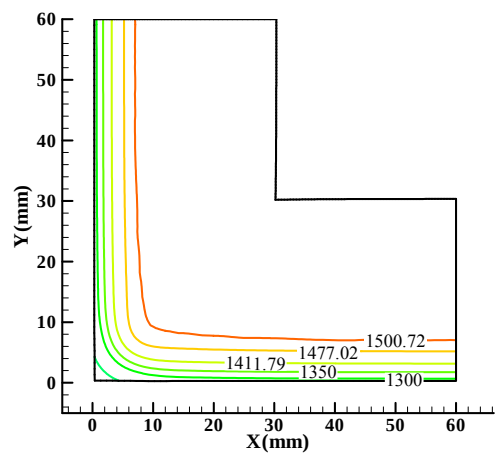

(b) 4.4m/min, 0.75% Linear Taper

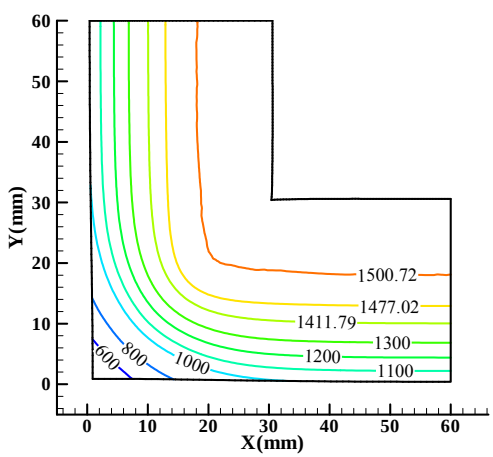

(c) 2.2m/min, Uniform Heat Flux

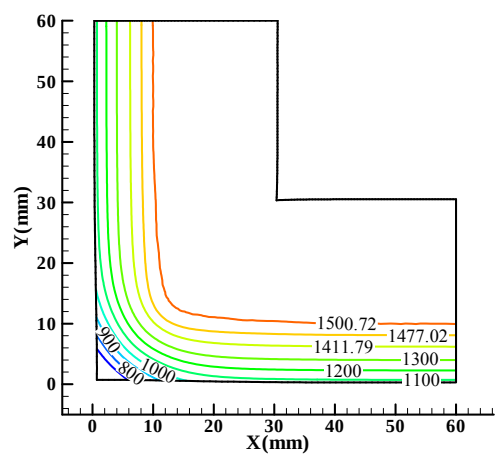

(d) 4.4 m/min, Uniform Heat Flux

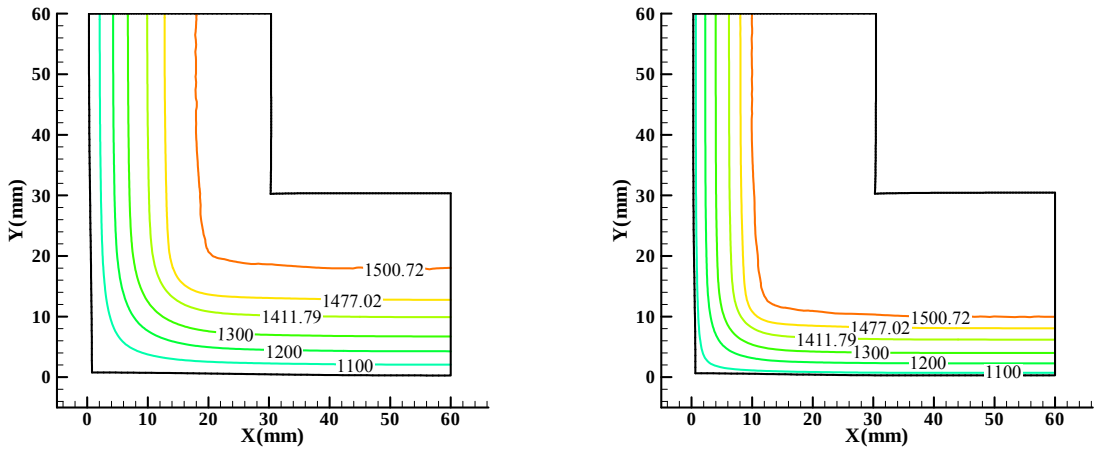

(e) 2.2m/min, Uniform Surface Temperature (f) 4.4 m/min, Uniform Surface Temperature

Figure 12: Temperature Contours at the Mold Exit

Both the mold configurations with uniform heat flux and uniform surface temperature around the mold perimeter produce a thicker shell near the corner relative to the shell near the face center. This is due to 2D cooling. The shell thicknesses at billet face center for the mold with 0.75% linear taper in Fig. (12a) and (12b) are much thinner than those with the mold providing the prescribed surface heat flux in Fig. (12c) and (12d) as well as the uniform surface temperature in Fig. (12e) and (12f). This indicates that 0.75%/m is much less than ideal taper at face center. This practical mold configuration also leads to a hot spot at the off-corner region at 2.2 m/min speed in Fig. (12a). This indicates that more taper is needed both in the top region of the mold and near the corners to avoid the hot spots.

Fig. (13) compares the surface temperature histories starting from the meniscus at the billet corner for the three different mold configurations described above. The traditionally believed optimal taper, which perfectly follows the shell shrinkage everywhere, and which corresponds to the uniform heat flux configuration, produces an extremely cold corner in the mold. When the billet leaves the mold, there is nearly 200 ^{o}C reheating near the corner despite the spray zone design to minimize surface temperature change at the billet face center. The corner cools faster than for the other two mold configurations due to 2D heat convection in the secondary cooling zone. Previous investigations of internal cracks [34, 35] suggest that reheating should be avoided to prevent internal cracks. Thus, an extremely cold corner is not favorable, which means that the traditional strategy for optimal taper design is not optimal near the corner.

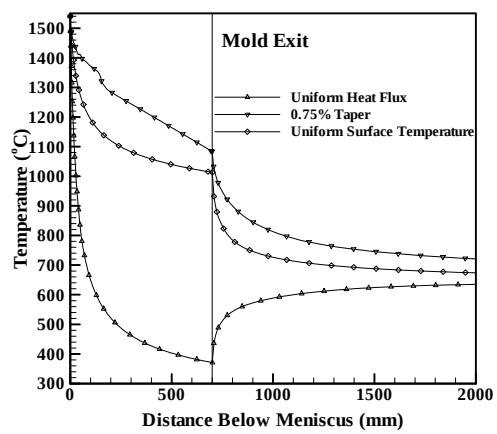

Figure 13: Surface Temperature Histories

Sub-Mold Bulging and Longitudinal Off-corner Sub-Surface Cracks

As the billet leaves the mold, ferrostatic pressure from the liquid core due to gravity is totally supported by the solidifying shell and produces sub-mold bulging. The amount of bulging is determined by the strength of the shell. A hot and thin shell having low strength will bulge more. The more severe creep at higher temperature makes the shell bulge even further. Fig. (14) shows the stress component along the shell surface with distorted shell for the billet casting in the mold with 0.75%/m linear taper at 100 mm below the mold exit. The amount of bulging is small while casting at 2.2 m/min (< 0.5 mm), but increases nearly 8 times when the casting speed

is doubled. The ferrostatic load bends the billet shell around the corner generating tensile stress along the solidifying front. This tensile stress is perpendicular to the growth direction of the dendrite arms and may lead to sub-surface cracks beneath the surface region about 10 ~ 15 mm from the corner. Recent experiments of steel strength near its melting temperature [36] indicates that the strength of plain carbon steel is around 10 MPa at 1300 ^{o}C which is the same as the maximum tensile stress value in Fig. (14b). This implies that fracture is highly possible around the sub-surface off-corner region in Fig. (14b). Fig. (15) shows the damage strain component along the solidification front which leads to hot tear cracks according to Eq. (6). The critical strain is calculated as 0.6% ~ 1% from Eq. (6). The damage strain at two off-corner regions near the solidification front exceeds the critical strain by over 60% when the casting speed is doubled to 4.4 m/min. This provides further evidence that hot tear cracks initiate for this condition. Therefore, a mold design with more taper to cool the corner is needed to avoid excessive bulging and longitudinal sub-surface off-corner cracks below the mold.

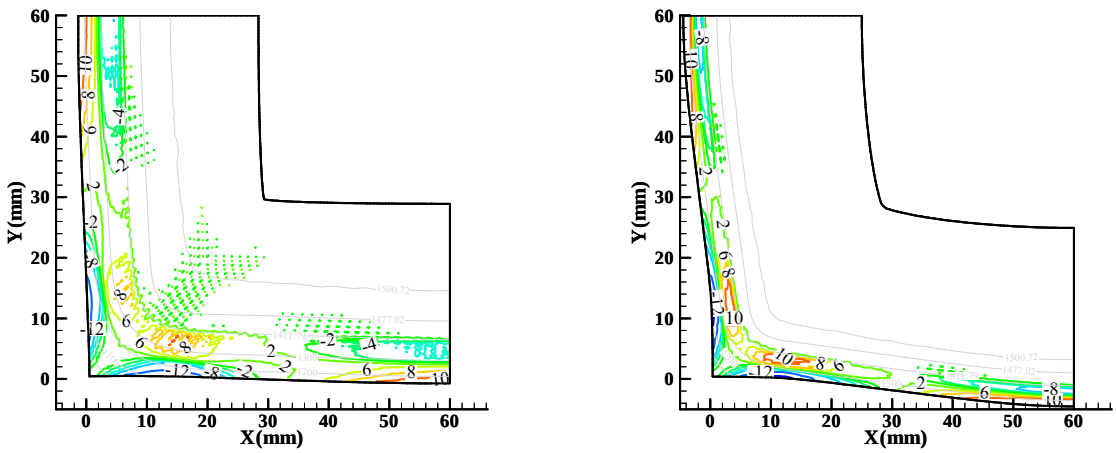

(a) 2.2m/min (b) 4.4 m/min

Figure 14: Stress Contours at 100 mm below Mold Exit

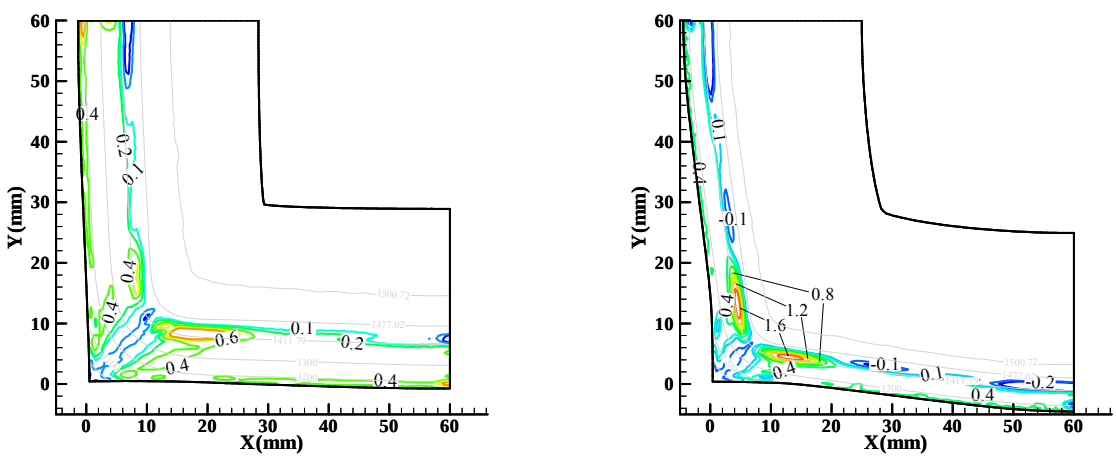

(a) 2.2m/min (b) 4.4 m/min

Figure 15: Damage Strain Contours at 100 mm below Mold Exit

Transverse Corner Cracks

Although a very cold corner may prevent bulging and off-corner cracks, it has its own shortcomings. A very cold corner in the mold will suffer reheating in the secondary cooling zone. Previous research by Grill [34] and Sorimachi [35] already indicated that reheating should be avoided to prevent sub-surface cracks. Fig. (16) shows the contours of the stress component along axial direction for the billet with the uniform heat flux around the perimeter at 100 mm below the mold exit. The corner is reheated from around 400 ^{o}C to 600 ^{o}C at this distance. The totally solidified steel near the surface tries to expand under reheating. This exerts tensile stress at the sub-surface region. Fig. (16) shows high tensile stresses at the corner sub-surface region. This high tensile stress region is closer to the solidification front at higher casting speed. Although the damage strain is not over the critical value for these speeds, it is believed that transverse sub-surface corner cracks would initiate when the casting speed is increased further.

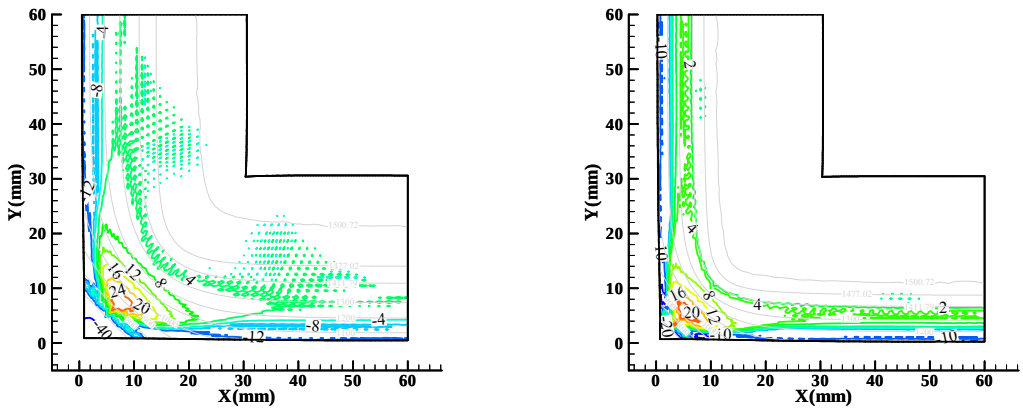

(a) 2.2m/min (b) 4.4 m/min

Figure 16: Axial Stress Contours at 100 mm below Mold Exit

Fig. (17) shows contours of the stress component along the billet axial direction for the billet with the uniform heat flux around the perimeter at two different locations (100 mm for 2.2 m/min and 200 mm for 4.4 m/min) below meniscus. Tensile stress up to 30 MPa near the corner surface is indicated. This is because the corner surface cools faster than its sub-surface layer. Transverse corner surface cracks are easily initiated under this stress state if the friction between the mold and the billet is considered, or if any other problems existed such as mold misalignment or stress concentration at deep oscillation marks. Thus, very cold corners should be avoided to prevent transverse corner surface cracks and sub-surface cracks.

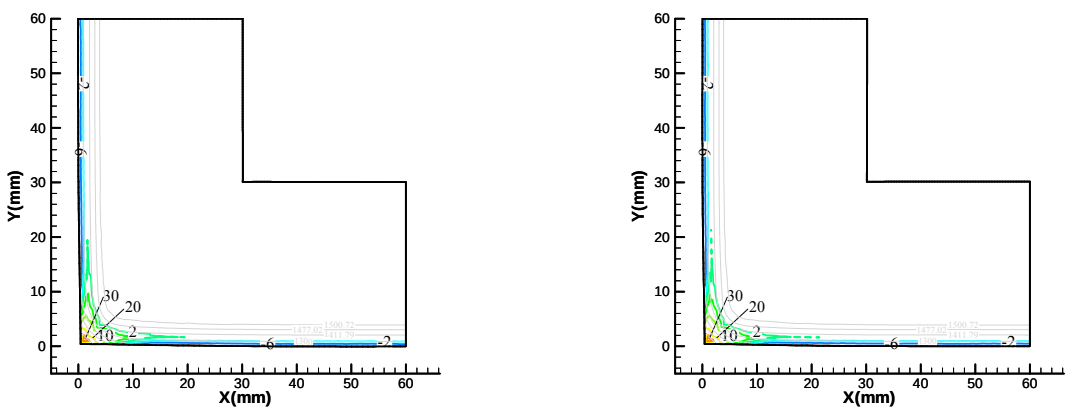

(a) 2.2m/min at 100 mm Below Meniscus (b) 4.4 m/min at 200 mm Below Meniscus

Figure 17: Axial Stress Contours

OPTIMAL TAPER PROFILE NEAR BILLET CORNER

It has been found that an optimal mold taper should avoid both very cold or very hot billet corners in order to avoid cracks or excessive bulging. Therefore, the optimal taper should have the following features:

1. It should be large enough to follow the shrinkage of the billet around the face center to avoid gap formation.
2. It should allow some amount of gap between the billet surface and the mold wall to offset the over cooling caused by 2D heat transfer near the billet corner so that the surface temperature of the billet is uniform around the perimeter. This is consistent with industrial practice that uses less taper near the corner [37].

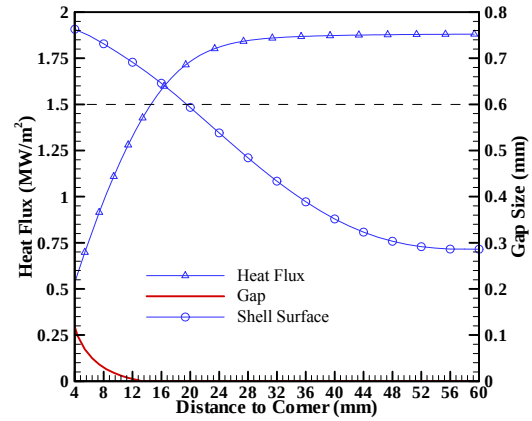

Figure 18: Shell Shrinkage, Heat Flux and Gap at the Mold Exit

Since some gap is needed near the billet corner, the optimal taper could not be determined by only analyzing billet shrinkage. Conditions of the heat flux profile near the corner as well as the heat resistance across the gap are also needed. This makes the optimal taper prediction much more complex. Fig. (18) shows the heat flux at the shell surface and the gap size near the corner at mold exit that are needed to achieve the uniform surface temperature around the mold perimeter. The heat flux is quite uniform away from the billet corner with its value described by Eq. (8). The heat flux drops near the corner to compensate the 2D heat transfer. The mold should be designed to leave a gap on the order of 0.1 mm between the billet and the mold from 13 mm from the corner in order to reduce the heat transfer. The optimal gap is only predicted up to 4 mm from the corner since the round corners of real molds were not modeled in this work. The dashed line indicates the ideal mold wall position predicted by the CON2D model with a numerically simple 1D slice domain. This 1D prediction is surprisingly accurate at the corner as it leaves a gap up to 0.15 mm even though it does not consider the corner effect totally. Fig. (19) shows the shrinkage of the billet under different assumptions of mold operation compared with the 0.75%/m linear taper case. The billet shrinkage profile with the uniform surface temperature compares closely to the ideal taper prediction of the 1D thermal stress model. Considering that the optimal taper should be less than the billet shrinkage to allow some gap near the billet corner, the ideal taper prediction of the 1D slice model is a reasonable estimation method.

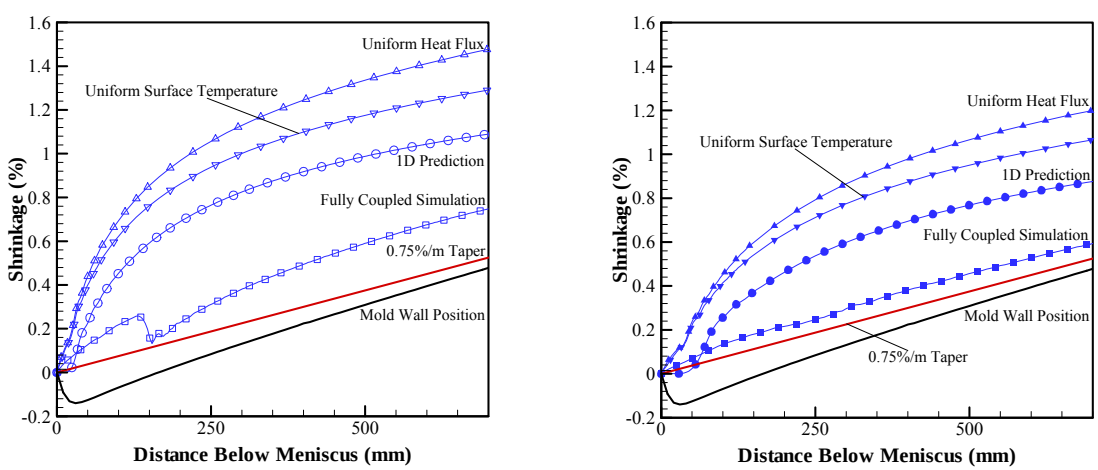

(a) 2.2m/min (b) 4.4 m/min

Figure 19: Optimal Taper Prediction

OPTIMAL TAPER PROFILES

The 1-D slice model of CON2D has been adopted to investigate the effects of casting speed and heat flux on optimal taper profile including the effects of the mold distortion. Details of the slice model are discussed elsewhere[21]. The shrinkage profiles of the billet are given in Fig. (20) up to 1000 mm assuming the average heat flux between the mold and the billet is only a function of dwell time as given in Eq. (7). It can be observed that the instantaneous taper is not linear. Larger taper is needed near the meniscus and for shorter molds. This is mainly due to the instantaneous heat flux profile. Heat flux is high near the meniscus and drops monotonically thereafter. Multifold linear taper or parabolic taper is recommended to prevent a general gap between the mold and billet surfaces near the meniscus. As the casting speed increases, the amount of mold taper should be reduced accordingly, due to less dwell time, the billet stays in the mold shorter which decreases the total heat extracted.

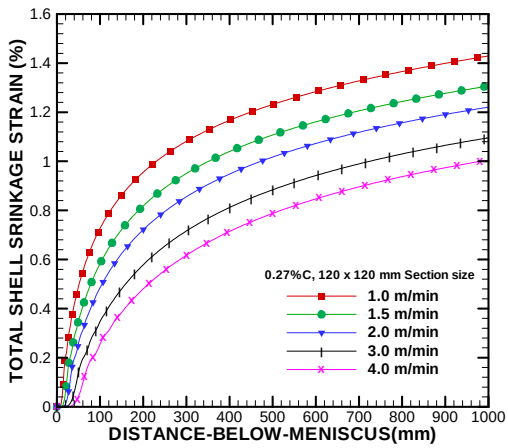

Figure 20: Optimal Taper Profiles Predicted By Slice Model

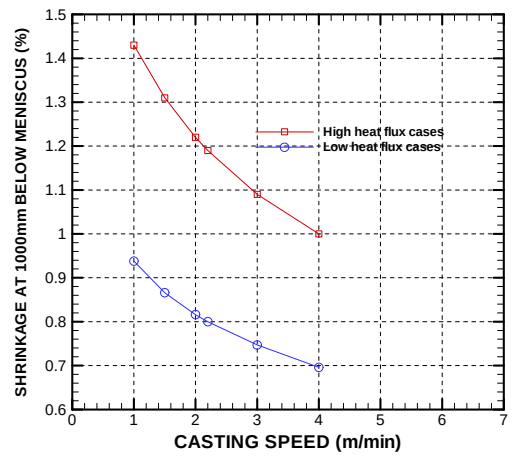

Figure 21: Shrinkage at 1000mm

Fig. (21) shows the shrinkage of the billet at 1000 mm below meniscus as a function of casting speed. The high heat flux curve corresponds to the heat flux profile fitted by Wolf [28] for billet casters, while the lower one corresponds to the heat flux profile fitted by C. Li [8]. These two profiles enclose most of the published average heat flux measurements for billet casters [28, 30]. Smaller taper is needed when the average heat flux in the mold is lower. It is also consistent to Fig. (20) that mold taper should be reduced as the casting speed increases.

Fig. (22) shows the shrinkage of the billet at mold exit as a function of the total heat extracted from the mold for different casting speeds and mold lengths. At each casting speed, the shrinkages are measured for different working mold lengths, 50 mm, 200 mm, 500 mm, 700 mm and 1000 mm. It is observed that the shrinkage depends on the total heat extracted by the mold only. The profiles for different casting speeds collapse into one profile, which indicates that the total heat removed in the mold is a more fundamental parameter controlling the amount of taper needed at the mold exit than either casting speed, or mold length. This important finding is true in general if the shape of the instantaneous heat flux profile stays the same for all different casting speeds.

Fig. (23) shows the maximum mold distortion at mold exit as a function of the average heat flux for different casting speeds and working mold lengths, based on Eq. (4). The profiles for different casting speeds again collapse to a single curve. This indicates the average heat flux in the mold is the fundamental parameter controlling the mold distortion. Mold distortion naturally increases with the average heat flux, owing to the higher mold temperature. This mold distortion should be taken into account when designing mold taper.

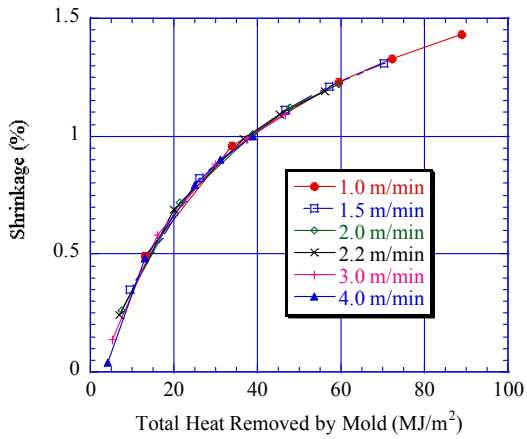

Figure 22: Shrinkage at Mold Exit vs. Total Heat Extracted by Mold

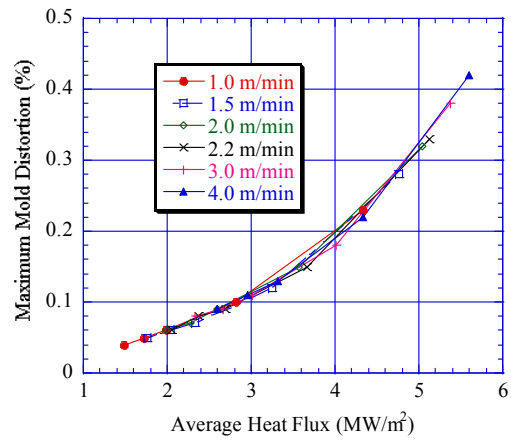

Figure 23: Maximum Mold Distortion vs. Average Heat Flux

CONCLUSIONS

A 2D thermal-mechanical model has been applied to investigate different mold configuration assumptions including corner behavior in order to predict optimal taper profiles. Several conclusions can be drawn:

- The shape of the mold wall around the billet perimeter should be carefully designed to ensure optimal thermal-mechanical behavior of the billet, especially near its corner. Too little taper leads to hot spot at off-corner location, and increases sub-mold bulging. Longitudinal off-corner sub-surface cracks or even breakouts may happen at extreme conditions. Too much taper overcools the corner region. This makes the billet prone to transverse surface cracks or longitudinal sub-surface cracks. The ideal taper design minimizes surface temperature differences around the billet perimeter.
- Although accurate taper prediction should consider a full 2D transverse section, a 1D taper prediction by CON2D with a slice domain is surprisingly accurate even for billet casting molds. Considering its great computational savings, this 1D method is acceptable for online taper prediction in industry or parametric studies in academia.
- The ideal taper is a function of casting speed and mold length. More fundamentally, it depends on the total heat removed in the mold regardless of the casting speed or mold length. The higher is the total heat extracted by the mold, the larger taper is needed. A 1.4%/m taper is needed when the total heat removed by mold is 90 MJ/m^2. When the total heat removed by mold is decreased to 10 MJ/m^2, almost no taper is needed.
- More taper is needed near the meniscus in order to compensate for the faster initial shrinkage. Therefore, parabolic mold taper or multifold linear taper with larger taper near the meniscus is recommended.
- Mold distortion away from shell increases the need for parabolic or multifold linear taper in billet molds. Mold distortion increases with heat flux in the mold from 0.04% at 1.4 MW/m^2 to over 0.4% at 5.6 MW/m^2.
- Further work is needed to investigate optimal mold taper profiles around the mold perimeter in addition to down its length.

ACKNOWLEDGEMENTS

The authors would like to thank the Continuous Casting Consortium of the University of Illinois for financial support. The authors also thank Ya Meng for help with the CON1D program and the National Center of Supercomputing and Applications (NCSA) for providing computing facilities and Don Lorento, Accumold, for helpful suggestions.

REFERENCES

1. R.J. Dippenaar, I.V. Samarasekera and J.K. Brimacombe, "Mold Taper in Continuous Casting Billet Machines," ISS Transactions, Vol. 7, 1986, 31.
2. J.E. Kelly, K.P. Michalek, T.G. O'Connor, B.G. Thomas, J.A. Dantzig, "Initial Development of Thermal and Stress Fields in Continuously Cast Steel Billets," Metall. Trans. A, Vol. 19A (10), 1988, 2589-2602.
3. J.H. Zietsman, S. Kumar, J.A. Meech, I.V. Samarasekera, J.K. Brimacombe, "Taper design in continuous billet casting using artificial neural networks," Ironmaking and Steelmaking, Vol. 25 (6), 1998, 476.
4. I.A. Bakshi, J.L. Brendzy, N. Walker, S. Chandra, I.V. Samarasekera, J.K. Brimacombe, "Mould-strand interaction in continuous casting of steel billets -- Part 1 Industrial trials, Part 2 Lubrication and oscillation mark formation, Part 3 Mould heat transfer and taper," Ironmaking and Steelmaking, Vol. 20 (1), 1993, 54.
5. S. Chandra, J.K. Brimacombe and I.V. Samarasekera, "Mould-strand interaction in continuous casting of steel billets, Part 3: Mould heat transfer and taper," Ironmaking and Steelmaking, Vol. 20 (2), 1993, 104.
6. C. Chow, I.V. Samarasekera, B.N. Walker, G. Lockhart, "High speed continuous casting of steel billets. Part 2: Mould heat transfer and mould design," Ironmaking and Steelmaking, Vol. 29 (1), 2002, 61-69.
7. J.K. Park, B.G. Thomas and I.V. Samarasekera, "Analysis of Thermal-Mechanical Behavior in Billet Casting with Different Mould Corner Radii," Ironmaking and Steelmaking, in press,
8. C. Li and B.G. Thomas, "Maximum Casting Speed for CC Steel Billets Based on Sub-mold Bulging Computation," 85th Steelmaking Conf., (Nashiville, TN), ISS-AIME, Warrendale, PA, Vol. 85, 2002, 109-130.
9. A. Moitra, "Thermo-Mechanical Model of Steel Shell Behavior in Continuous Slab Casting," Ph.D. Thesis Thesis, UIUC, 1993.
10. H. Zhu, "Coupled Thermal-Mechanical Finite-Element Model with Application to Initial Solidification," Ph.D. Thesis Thesis, UIUC, 1996.
11. E. Lemmon, "Multi-dimentional Integral Phase Change Approximations for Finite-Element Conduction Codes," in Numerical Methods in Heat Transfer, Vol. 1, R.W. Lewis, K. Morgan and O.C. Zienkiewicz, eds., John Wiley & Sons, 1981, 201-213.
12. Y.M. Won and B.G. Thomas, "Simple Model of Microsegregation during Solidification of Steels," Metallurgical and Materials Transactions A, Vol. 32A (July, 2001), 2001, 1755-1767.
13. P.F. Kozlowski, B.G. Thomas, J.A. Azzi, H. Wang, "Simple Constitutive Equations for Steel at High Temperature," Metall. Trans. A, Vol. 23 (March), 1992, 903-918.
14. J.-C.T. Parkman, "Simulation of Thermal Mechanical Behavior During Initial Solidification of Steel," Master Thesis Thesis, UIUC, 2000.
15. P.J. Wray, "Plastic Deformation of Delta-Ferritic Iron at Intermediate Strain Rates," Metall. Trans. A, Vol. 7A (November), 1976, 1621-1627.
16. P.J. Wray, "Effect of Crabon Content on the Plastic Flow of Plain Carbon Steels at Elevated Temperatures," Metall. Trans. A, Vol. 13A (January), 1982, 125-134.
17. T. Suzuki, K.H. Tacke, K. Wunnenberg, K. Schwerdtfeger, "Creep Properties of Steel at Continuous Casting Temperatures," Ironmaking and Steelmaking, Vol. 15 (2), 1988, 90-100.
18. K. Harste, "Investigation of the shrinkage and the origin of mechanical tension during the solidification and successive cooling of cylindrical bars of Fe-C alloys," Ph.D. Dissertation Thesis, Technical University of Clausthal, 1989.
19. A. Jablonka, K. Harste and K. Schwerdtfeger, "Thermomechanical properties if iron and iron-carbon alloys: density and thermal contraction," Continuous Casting, Vol. 9, 1997, 155.
20. I. Jimbo and A. A. W. Cramb, "The Density of Liquid Iron--Carbon Alloys," Metallurgical Transactions B (USA), Vol. 24B (1), 1993, 5-10.
21. C. Ojeda and B.G. Thomas, "Ideal Taper Prediction For Slab Casting," ISSTech 2003, (Indianapolis, IN), ISS, Warrendale, PA, 2001, 2003.

22. Y. Won, T.-J. Yeo, D. Seol, K. Oh, "A New Criterion for Internal Crack Formation in Continuously Cast Steels," Metall. Trans. B, Vol. 31B (4), 2000, 779~794.
23. J.H. Weiner and B.A. Boley, "Elasto-Plastic Thermal Stresses in A Solidifying Body," J. Mech. Phys. Solids, Vol. 11, 1963, 145-154.
24. E. Howard and D. Lorento, "Development of High Speed Casting," 1996 Electric Furnace Conference Proceedings, (Dallas, TX), 1996, 353-358.
25. J.K. Park, C. Li, B.G. Thomas, I.V. Samarasekera, "Analysis of Thermo-Mechanical Behavior In Billet Casting," 60th Electric Furnace Conference, (San Antonio, TX), ISS, Warrendale, PA, 2001, Vol. 60, 2002, 17.
26. Y. Meng and B.G. Thomas. Heat Transfer and Solidification Model of Continuous Slab Casting: CON1D. Metall. Trans B. (2002),
27. C. Li and B.G. Thomas, "Analysis of the Potential Productivity of Continuous Cast Molds," Brimacombe Memorial Symposium, (Vancouver, Canada), Canadian Inst. Min. Metall., 2000, 17, 201.
28. M.M. Wolf, "Mold Length in Slab Casting - A Review," Ironmaking and Steelmaking, Vol. 23 (2), 1996, 47-51.
29. J.K. Park, I.V. Samarasekera, B.G. Thomas, U.S. Yoon, "Analysis of Thermal and Mechanical Behavior of Copper Mould During Thin Slab Casting," 83th Steelmaking Conference Proceedings, (Pittsburgh, PA), Iron and Steel Society, Vol. 83, 2000, 9-21, 061.
30. N. Kapaj, M. Pavlicevic and A. Poloni, "Exceeding the casting speed of bloom CC machines by three times," 84th Steelmaking Conference, (Baltimore, MD), Iron and Steel Society/AIME, Warrendale, PA, Vol. 84, 2001, 67-78, 222.
31. J.K. Brimacombe, "Design of continuous casting machines based on a heat-flow analysis: state-of-the-art review," Canadian Metall. Quarterly, Vol. 15 (2), 1976, 163-175.
32. I.V. Samarasekera, "High Speed Casting of High Quality Billets," Report, University of British Columbia, 1998.
33. J.K. Brimacombe, P.K. Agarwal, L.A. Baptista, S. Hibbins, B. Prabhakar, "Spray Cooling in the Continuous Casting of Steel," ISS, Iron and Steel Society, Inc., Warrendale, PA, Vol. 2, 1984, 105-123, 101.
34. A. Grill, J.K. Brimacombe and F. Weinberg, "Mathematical Analysis of Stresses in Continuous Casting of Steel," Ironmaking Steelmaking, Vol. 3 (1), 1976, 38-47.
35. K. Sorimachi and J.K. Brimacombe, "Improvements in Mathematical Modelling of Stresses in Continuous Casting of Steel," Ironmaking Steelmaking, Vol. 4 (4), 1977, 240-245.
36. H. Mizukami, A. Yamanaka and T. Watanabe, "High Temperature Deformation Behavior of Peritectic Carbon Steel During Solidification," ISIJ International, Vol. 42 (9), 2002, 964-973.
37. D. Lorento, "Billet Mold Taper and Secondary Cooling Pattern Design", personal communication, 2002.